

Received: 2014.05.22
Accepted: 2014.06.20
Published: 2014.10.15

Application of F-18-Sodium Fluoride (NaF) Dynamic PET-CT (dPET-CT) for Defect Healing: A Comparison of Biomaterials in an Experimental Osteoporotic Rat Model

Authors' Contribution:
Study Design A
Data Collection B
Statistical Analysis C
Data Interpretation D
Manuscript Preparation E
Literature Search F
Funds Collection G

ABCDEF 1 **Caixia Cheng**
B 2 **Volker Alt**
C 1 **Leyun Pan**
B 2 **Ulrich Thormann**
G 2 **Reinhard Schnettler**
A 1 **Ludwig G. Strauss**
F 3 **Sascha Heinemann**
B 4 **Matthias Schumacher**
G 4 **Michael Gelinsky**
D 5 **Berthold Nies**
ACG 1 **Antonia Dimitrakopoulou-Strauss**

1 Clinical Cooperation Unit Nuclear Medicine, German Cancer Research Center, Heidelberg, Germany
2 Department of Trauma Surgery, University Hospital Giessen-Marburg GmbH, Giessen, Germany
3 Max-Bergmann-Center of Biomaterials, Institute of Materials Science, Technische Universität Dresden, Dresden, Germany
4 Technische Universität Dresden, Centre for Translational Bone, Joint and Soft Tissue Research, Medical Faculty and University Hospital Carl Gustav Carus, Dresden, Germany
5 InnoTERE GmbH, Radebeul, Germany

Corresponding Author: Caixia Cheng, e-mail: c.cheng@dkfz.de

Source of support: This study is part of the Sonderforschungsbereich-Transregio 79 (SFB-TR 79) and was in part financially supported by the Deutsche Forschungsgemeinschaft (German Research Foundation, DFG)

Background: The aim of the current study was to measure and compare the effect of various biomaterials for the healing of osteoporotic bone defects in the rat femur using ¹⁸F-sodium fluoride dPET-CT.


Material/Methods: Osteoporosis was induced by ovariectomy and a calcium-restricted diet. After 3 months, rats were operated on to create a 4-mm wedge-shaped defect in the distal metaphyseal femur. Bone substitution materials of calcium phosphate cement (CPC), composites of collagen and silica, and iron foams with interconnecting pores were inserted. Strontium or bisphosphonate, which are well known for having positive effects in osteoporosis treatment, were added into the materials. Eighteen weeks after osteoporosis induction and 6 weeks following femoral surgery, dPET-CT studies scan were performed with ¹⁸F-Sodium Fluoride. Standardized uptake values (SUVs) and a 2-tissue compartmental learning-machine model (K1-k4, vessel density [VB], influx [ki]) were used for quantitative analysis.

Results: k3, reflecting the formation of fluoroapatite, revealed a statistically significant increase at the biomaterial-bone interface due to the Sr release from strontium-modified calcium phosphate cement (SrCPC) compared to CPC, which demonstrated enhanced new bone formation. In addition, k3 as measured in the porous scaffold silica/collagen xerogel (Sc-B30), showed a significant increase based on Wilcoxon rank-sum test (p<0.05) as compared with monolithic silica/collagen xerogel (B30) in the defect region. Furthermore, ki, reflecting the net plasma clearance of tracer to bone mineral measured in the iron foam with coating of the bisphosphonate zoledronic acid (Fe-BP), was enhanced as compared with plain iron foam (Fe) in the defect region.

Conclusions: k3 was the most significant parameter for the characterization of healing processes and revealed the best differentiation between the 2 different biomaterials. PET scanning using ¹⁸F-sodium fluoride seems to be a sensitive and useful method for evaluation of bone healing after replacement with these biomaterials.

MeSH Keywords: **Aortopulmonary Septal Defect • Biomarkers, Pharmacological • Osteoporosis**

Full-text PDF: <http://www.medscimonit.com/abstract/index/idArt/891073>

 3807

 2

 4

 33



Background

Therapy for osteoporotic fractures remains a critical challenge. Research interest is increasing in biomaterials with the potential to stimulate bone healing have gained interest to improve treatment outcome for patients with osteoporotic fractures [1]. Calcium phosphate cements (CPC) has been used in bone surgery for many years [2,3]. The bio-inspired combination of the inorganic component silica and the organic component collagen has led to a novel class of innovative biomaterials because silica and collagen turned out to be ideal partners for composite formation, resulting in advantageous synergistic effects in material properties suitable for soft-tissue or hard-tissue substitution applications. The chemical and technological flexibility of the silica/collagen system has generated a remarkably wide range of biomaterials individually adapted for a large number of biomedical applications [4], including soft hydrogels [5], macroporous scaffolds [6], and solid compact xerogels [7]. In addition, metal foams open new opportunities for design of bone implants due to their mechanical stability [8]. In cardiovascular applications, iron has been used successfully in animal implantation studies and in clinical cases [9]. Iron has relatively long degradation timeframes, which are particularly needed in bone surgery [10].

The use of PET scanning as a diagnostic tool for fracture healing is attractive because it can provide a direct quantitative assessment of metabolic activity in a region of interest. We recently showed that the fixation of fluoride in the bone matrix may be enhanced using CPC, especially CPC with strontium carbonate as biomaterial for bone replacement and defect healing in osteoporotic bone [11]. The present study was designed to examine the efficacy of multifunctional bioabsorbable implants, including CPC-based, silica/collagen-based, and iron-based composites for the treatment of experimental osteoporotic fractures. The treatment response was assessed by F-18-sodium fluoride (NaF) dynamic PET-CT (dPET-CT).

Material and Methods

Ethics statement

All animal procedures were carried out in accordance with the Guide for Care and Use of Laboratory Animals of the National Institutes of Health. The animal studies were approved by the corresponding authority (Regierungspräsidium Gießen, GI 20/28 Nr. 92/2009).

Animal characteristics, operative protocol

The study included 65 3-month-old female Sprague-Dawley rats (Charles Rivers Wiga, Sulzbach, Germany) with a body weight

between 250 and 400 g. After an acclimatization of 4 weeks, an osteoporotic bone status was induced by bilateral ovariectomy and a calcium-, phosphorous-, vitamin D3-, soy-, and phytoestrogen-free diet, as previously described by Heiss et al. [12]. After 3 months, the animals underwent femur surgery under general anaesthesia with xylazine (4 mg/kg body weight⁻¹, Rompun®, Bayer) and ketamine (100 mg/kg body weight⁻¹, Hostaket®, Hoechst) by intraperitoneal injection. Details of the femur surgery have been described by Alt et al. [13]. The left femur was disinfected with povidone iodine (Braunol®, Braun, Melsungen, Germany) and draped in a sterile manner. After making a 4-cm skin incision at the lateral aspect of the distal thigh, the lateral vastus muscle and the lateral head of the femoral biceps muscle were dissected in their septum intermusculare and the femur from shaft to the condyle massif was exposed. Subsequently, a 7-hole T-shaped miniplate (Leibinger® XS-miniplate, Stryker®, Schönkirchen, Germany) was slightly bent and fixed to the lateral femur with 1.2-mm screws. Afterwards, a wedge-shaped defect with a lateral height of 4 mm was then created at the metaphyseal area of the femur. The cutting lines were marked with a custom-made triangular sawing guide with a lateral length of 4 mm. The distal transverse osteotomy was made just above the border of the femoropatellar joint, without bruising the articular cartilage. Cutting was performed with a water-cooled oscillating saw.

Bone substitution materials

Calcium phosphate cement (CPC) and CPC enriched with strontium (SrCPC) were prepared as described previously [11,14]. In brief, CPC powder was composed of α -tricalcium phosphate (α -Ca₃(PO₄)₂), calcium hydrogen phosphate (CaHPO₄), calcium carbonate (CaCO₃), and hydroxyapatite (Ca₁₀(PO₄)₆(OH)₂), and was supplied by InnoTERE GmbH (Radebeul, Germany). SrCPC powder was obtained by substitution of CaCO₃ by SrCO₃ (Alfa Aesar) in the CPC cement precursor powder. Sr-modification resulted in a total Sr content of 2.21%. A mouldable paste was obtained by mixing the cement powder with Na₂HPO₄ solution using a liquid-to-powder ratio of 500 and 350 μ l/g for CPC and SrCPC, respectively, immediately prior to implantation. SrCPC was previously shown to release significant amounts of Sr²⁺ upon immersion in aqueous media (e.g., cell culture medium) and to positively influence both *in vitro* osteoblast proliferation and differentiation and *in vivo* bone formation [15]. Composites of silica and fibrillar bovine collagen were used for implantation as monolithic xerogels (B30, 70 wt% silica, 30 wt% collagen) or as porous scaffold (Sc-B30, Xerogel particles B30, size <250 μ m, embedded in a collagen matrix with xerogel/matrix weight ratio of 1.0) [16]. For preparation of compact silica/collagen xerogels, bovine tropocollagen type I (GfN, Germany) was dialysed (Nominal Molecular Weight Cut-Off 12-14 kDa, Roth, Germany) against deionized water followed by fibrillation in 30-mM neutral sodium phosphate buffer solution, lyophilisation

Table 1. The information of biomaterials and number of animals used in this study.

Group	Biomaterials	Number of animals
Control	/	7
CPC	Calcium phosphate cement (α TCP-based)	7
SrCPC	CPC with 8.36 wt% strontium (Sr/Ca=0.123)	7
B30	Monolithic xerogels (70 wt% silica, 30 wt% collagen)	7
Sc-B30	Scaffolds xerogel particles B30	7
Sc-B30Sr20	Scaffolds xerogel particles (50 wt% silica, 30 wt% fibrillar bovine collagen, and 20 wt% strontium carbonate)	8
Fe	Iron foam	7
Fe-S	Iron foam with strontium	7
Fe-BP	Iron foam with zoledronic acid	8

(Christ Alpha 1-4 laboratory freeze-dryer, Osterode, Germany), and resuspension in 0.1 M TrisHCl pH 7.4 (Roth) to obtain homogeneous 30 mg/ml suspensions [8]. The silica component was prepared by hydrolysing tetraethoxysilane (TEOS, 99%, Sigma, Germany; molar ratio TEOS/water=1/4) under acidic conditions (0.01 M HCl) to obtain silicic acid. Vigorous stirring of calculated volumes of silicic acid and collagen suspension to obtain a final composition of 70% silica and 30% collagen (B30) resulted in the formation of 800- μ l hydrogels. A modification of the scaffolds was prepared by using xerogel particles consisting of 50 wt% silica, 30 wt% fibrillar bovine collagen, and 20 wt% strontium carbonate (Sc-B30Sr20). Strontium carbonate was introduced as a third phase by being previously added to the collagen suspension. B30 or B30Sr20 gels were transferred to molds, stabilized, and dried for 7 days in an Espec SH-221 climate chamber (Japan) at 37°C and 95% relative humidity. The resulting xerogel samples were ground and classified according to the particle size. On the one hand, B30 xerogel particles <0.250 mm were compacted using a custom-made pressing tool to obtain monolithic B30 xerogel samples exhibiting exactly the above-described bone defect shape. On the other hand, B30 or B30Sr20 xerogel particles <0.120 mm were added to a 30-mg/ml collagen suspension adjusting a xerogel/collagen weight ratio of 1/1. These xerogel particle/collagen suspensions were transferred to custom-made silicon molds to again obtain the above-described bone defect shape, cooled at 0.5 K/min to -20°C (Espec SH-221 climate chamber, Osaka, Japan) followed by lyophilisation (Christ Alpha 1-4 laboratory freeze-dryer, Osterode, Germany). The scaffolds were chemically cross-linked by immersing in 1 wt% N-(3-dimethylaminopropyl)-N0-ethylcarbodiimide (EDC)/N-hydroxysuccinimide (NHS) (Sigma) in 40% ethanol for 24 h. Finally, the scaffolds were rinsed in deionized water and freeze-dried again. According to the xerogel particle composition used,

scaffold sample labels were ScB30 or ScB30Sr20, respectively. All xerogel or scaffold samples were gamma-sterilized at 25 kGy before used for implantation.

Moreover, iron foam with interconnected pores (Fe) was applied. For preparation of strontium coating of iron foams, 153 mL of ultrapure water and 17 mL of phosphoric acid (85% H₃PO₄) were added in a 250-mL glass bottle. Strontium carbonate was then added carefully into the solution due to gas evolution. The solution was stirred on a magnetic stirrer for 1 h and settled overnight. The supernatant was diluted 20-fold using ultrapure water, which yielded the solution of Sr(H₂PO₄)₂. Ten Fe foams eroded and cleaned by IFAM (Fraunhofer Institute for Manufacturing Technology and Advanced Materials, Dresden) with an average weight of 170 mg were coated by suspension in 100 mL of Sr(H₂PO₄)₂ solution for 4 h under vacuum. Sr-coated foams were settled in fresh coating solution for another 3 days at room temperature and rinsed 3 times using absolute ethanol with subsequent drying at 40°C in a drying cabinet. Sr-coating resulted in an average weight gain of 37 mg or approximately 22%. In addition, the alloy element phosphorus is added with Fe3P-powder (Atmix, Japan) with a particle size of 3.8 μ m. To achieve a phosphate ratio of 0.6%, we added 3.8% of Fe3P powder. The iron foam was coated with zoledronic acid (Fe-BP) that is a member of the bisphosphonate family. Fe-BP was created by precipitation of zoledronic acid, stearate, and iron. Then the complex was carefully washed, dried, ground, and finally led to a coating of 35- μ g zoledronic acid, the basic iron foam. Open-cell metal foams are produced by a powder-metallurgical replication technique [17]. These 8 different formulations of bone substitution materials were implanted in the current animal model (n=7-8) (Table 1). A control group of 7 rats without any biomaterial was used as reference.

PET, kinetic model

Eighteen weeks after induction of osteoporosis and 6 weeks after femoral surgery, dPET-CT with ^{18}F -sodium fluoride (NaF) scans were performed. During scanning, rats were anesthetized using a mixture of nitrous oxide (1 l/min), oxygen (0.5 l/min) and isoflurane (1.5 vol.%).

dPET-CT studies were performed for 60 min after the intravenous application of 20 to 40 MBq ^{18}F -Sodium Fluoride, using a 28-frame protocol (10 frames of 30 s, 5 frames of 60 s, 5 frames of 120 s, and 8 frames of 300 s). A dedicated PET-CT system (Biograph™ mCT, 128 S Siemens Co, Erlangen, Germany) with an axial field of view of 21.6 cm with TrueV and TruePoint, operated in a 3-dimensional mode, was used for all animal studies. The system provides the simultaneous acquisition of 369 transverse PET slices with a slice thickness of 0.6 mm. Two rats were examined in parallel and were positioned in the axial plane of the system to maintain the optimum resolution in the center of the system. A high-resolution CT scan was performed prior the PET scanning with 160 mA, 80 kV, pitch of 0.85 cm in addition to the low-dose attenuation CT (80 mA, 80 kV) for attenuation correction of the acquired dynamic emission PET data. All PET images were attenuation-corrected and an image matrix of 400×400 pixels was used for iterative image reconstruction (voxel size 1.565×1.565×0.6 mm) based on the syngo MI PET/CT 2009C software version. The reconstructed images were converted to standardized uptake value (SUV) images based on the formula (18): $\text{SUV} = \text{tissue concentration (Bq/g)} / [\text{injected dose (Bq)} / \text{body weight (g)}]$. The SUV images 55–60 min post-injection were used for the assessment. The SUV images were generally used for all further quantitative evaluations.

dPET-CT data were evaluated using a dedicated software package [19,20]. Volumes of Interest were placed over the created defect area in the femur, and rotated PET images according to the CT images. A volume of interest consists of several regions of interest over the target area. Irregular regions of interest were drawn manually according to the fused PET-CT images, as mentioned before [11]. To precisely select the region to draw the VOI of the created defect, the fusion of PET images and CT scans by co-registration preprocessing was performed after rotation of each rat individually. First, we rotated the CT series to determine the optimum angle for the visualisation of the complete defect and the adjacent metal plates in the longitudinal direction. Then we used the same parameter settings for the rotation of the PET images. The next step was to fuse CT and PET and to use these fused images for the quantitative PET evaluation. The spatial resolution was 2 mm for PET image and 0.33 mm for CT image. The VOI for the defect was placed between the 2 screws located at the left and the right side of the 4-mm created defect. For input, we used

10 contiguous PET slices in the middle and lower third of the aorta. We avoided using the upper part of the thoracic aorta due to spillover from the heart. Compartmental modeling was used to gain a detailed quantitative evaluation of tracer kinetics. Herein, a 2-tissue compartment model was used to evaluate the dynamic studies and to gain quantitative data about the kinetics.

In the current study, the learning-machine 2-tissue compartment model was used for the fitting, and provided 5 parameters: the plasma clearance to the bone extracellular fluid (ECF) compartment and the rate constant for return of tracer to plasma; K_1 and k_2 ; the rate constants describing movement of tracer into and out of the bound bone compartment; k_3 and k_4 ; and the fractional blood volume, also called vessel density (VB), which reflects the amount of blood in the VOI. Following compartment analysis, we calculated the plasma clearance of tracer to bone mineral from the compartment data using the formula: $\text{influx (ki)} = (K_1 * k_3) / (k_2 + k_3)$. Compared to the standard iterative method, the machine learning method has the advantage of a fast convergence and avoidance of over-fitting [21]. The model parameters were accepted when K_1 – k_4 was less than 1 and VB exceeded 0. The unit for the rate constants K_1 – k_4 was 1/min.

Besides the compartmental analysis, a noncompartmental model based on the fractal dimension was used. The fractal dimension is a parameter of heterogeneity and was calculated for the time-activity data of each individual volume of interest. The values for fractal dimension vary from 0 to 2, showing the deterministic or chaotic distribution of tracer activity. We used a subdivision of 7×7 and a maximal SUV of 20 for the calculation of fractal dimension [22]. More details on the methodology used were published elsewhere [23].

Statistical analysis

Statistical evaluation was performed with Stata/SE 11.1 (StataCorp, College Station, TX, USA) using the descriptive statistics and box plots. Linear discriminant analysis was performed for calculating the sensitivity, specificity, positive predictive value (PPV), negative predictive value (NPV) and highest accuracy. The 2-sided Wilcoxon rank sum test was applied for all PET parameters, which also included SUV, using a single parameter analysis to assess groups. The significance level was set to $p < 0.05$.

Results

CPC based implants

We have reported that k_3 was the most sensitive PET parameter for the characterization of healing process and revealed the best differentiation for the empty defect and the

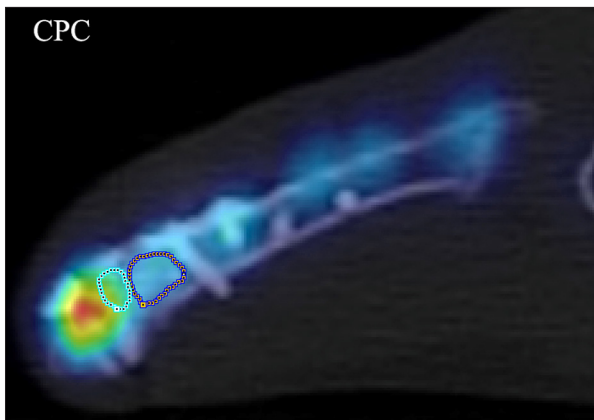


Figure 1. A representative 2D fused PET-CT image from the CPC group demonstrates how VOIs of the biomaterial-bone interface were drawn (left). The right VOI is CPC in the defect, and the accumulation of ^{18}F -sodium fluoride is primarily confined to the knee joints.

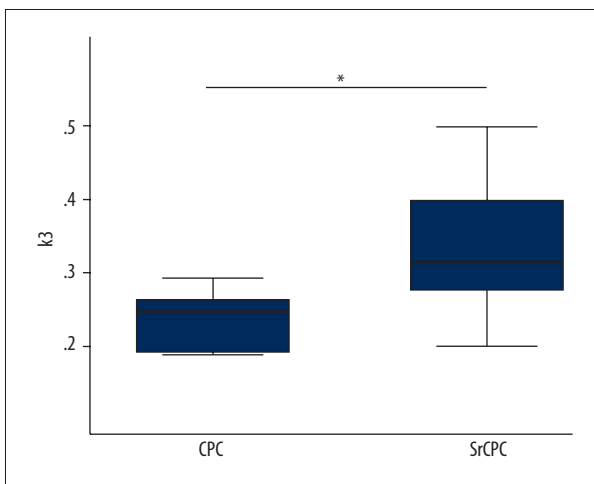


Figure 2. Box plots showing the PET parameter k_3 in the CPC and SrCPC group in the biomaterial-bone interface ($p=0.018$). * p value <0.05 was considered statistically significant.

CPC group, as well as the SrCPC, for the defect region [11]. However, no PET parameter demonstrated a significant difference between the CPC and SrCPC group in the defect region. In this study, the volume of interest (VOI) of the biomaterial-bone interface was selected for evaluation (Figure 1). The accumulation of ^{18}F -sodium fluoride is primarily confined to the knee joints. k_3 showed a statistically significant increase in the bone formation for the SrCPC group compared to the CPC group ($p=0.018$) in the biomaterial-bone interface (Figure 2).

Composites of silica and collagen

Three types of the composites were used: monolithic xerogels (B30) and porous scaffolds (Sc-B30 and Sc-B30Sr20).

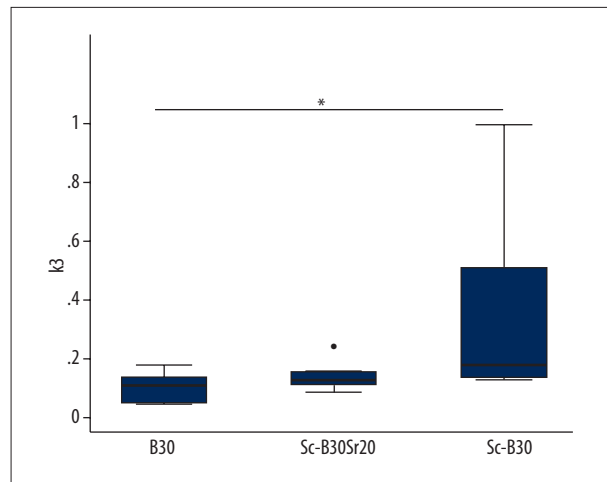


Figure 3. Box plots showing the PET parameter k_3 in the B30, Sc-B30 and Sc-B30Sr20 group in the defect ($p=0.022$). The dot on Sc-B30Sr20 is an outside value. * p value <0.05 was considered statistically significant.

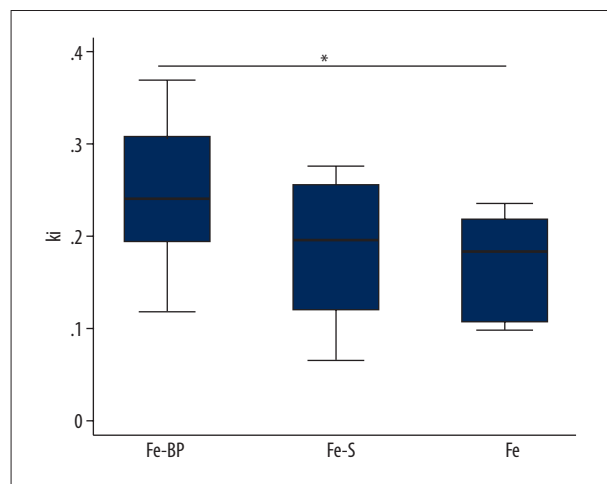


Figure 4. Box plots showing the PET parameter k_i in the Fe, Fe-S and Fe-BP group in the defect ($p=0.037$). * p value <0.05 was considered statistically significant.

Comparing the PET parameters, we could not detect significant changes between the 3 composites and the empty defect for both ROIs. Only k_3 in the Sc-B30 group exhibited a significant increase in comparison to the B30 group in the defect region (Figure 3, $p=0.022$).

Iron foam implants

Three different formulations of the iron foam were used as implants in the different rat groups: a) plain iron foam (Fe), b) strontium functionalized iron foam (Fe-S), c) iron foam with coating of the bisphosphonate zoledronic acid (Fe-BP). No significant differences were found in the PET parameters between the 3 implants and the empty defect for both ROIs.

Table 2. The classification results between two different groups in the defect region based on SVM_RFE with highest accuracy.

Group	Parameters	Accuracy	Sensitivity	Specificity	PPV	NPV
CPC vs. CPCSr	k3	11/14 (78.6%)	6/8 (75.0%)	5/6 (83.3%)	6/7 (85.7%)	5/7 (71.4%)
B30 vs. Sc-B30	k3, ki	12/13 (92.3%)	7/8 (86.3%)	5/5 (100.0%)	7/7 (100.0%)	5/6 (83.3%)
B30 vs. Sc-B30Sr20	VB, k3	11/14 (78.6%)	8/11 (72.7%)	3/3 (100.0%)	8/8 (100.0%)	3/6 (50.0%)
Sc-B30 vs. Sc-B30Sr20	K1, k3, ki, SUV	13/15 (86.7%)	6/7 (85.7%)	7/8 (86.3%)	6/7 (85.7%)	7/8 (86.3%)
Fe vs. Fe-S	k3, VB	11/15 (73.3%)	5/7 (71.4%)	6/8 (75.0%)	5/7 (71.4%)	6/8 (75.0%)
Fe vs. Fe-BP	VB, ki	12/15 (80.0%)	5/6 (83.3%)	7/9 (77.8%)	5/7 (71.4%)	7/8 (86.3%)
Fe-S vs. Fe-BP	VB, K1, k3, ki, SUV	12/16 (75.0%)	6/8 (75.0%)	6/8 (75.0%)	6/8 (75.0%)	6/8 (75.0%)

However, there was a significant increase of ki in the Fe-BP group as compared with the Fe group for the defect region (Figure 4, $p=0.037$).

Multiparameter analysis

A multiparameter analysis was performed to find differences between the 2 different groups based on the dPET-CT data. A linear discriminant analysis was used for classification. The aim was to identify a combination of variables that best discriminate each group of rats with different biomaterials in the defect region. An overall accuracy of >75% was achieved for the combination of some kinetic parameters between the 2 different groups. Furthermore, all sensitivity and specificity values from the multiparameter analysis were high (>71%) (Table 2). The highest overall accuracy of 78.6% was achieved for k3 between the CPC and SrCPC group based on the biomaterial-bone interface. The positive predictive value (NPV) and the negative predictive value (PPV) were 85.7% and 71.4%, respectively. Therefore, 6/7 rats with CPC in the defect and as 5/7 rats with SrCPC in the defect could be correctly classified based on the k3 as measured.

Between the Sc-B30 and Sc-B30Sr group, the highest overall accuracy of 86.7% was achieved for a combination of K1, k3, ki, and SUV. We could correctly classify 7/8 rats with Sc-B30 in the defect (NPV of 86.3%) and 6/7 rats with Sc-B30Sr (PPV of 85.7%). Between the Sc-B30 and B30 group, the highest overall accuracy of 92.3% was achieved for a combination of k3 and ki. We could correctly classify 5/6 rats with B30 in the defect (NPV of 83.3%) and 7/7 rats with Sc-B30 (PPV of 100%). Between the Sc-B30Sr20 and B30 group, the highest overall accuracy of 78.6% was achieved for a combination of k3 and VB. We could correctly classify 3/6 rats with B30 in the defect (NPV of 50.0%) and 8/8 rats with Sc-B30Sr20 (PPV of 100%).

Between the Fe and Fe-S group, the 73.3% highest overall accuracy was achieved for a combination of k3 and VB. We could correctly classify 6/8 rats with Fe-S in the defect (NPV

of 75.0%) and 5/7 rats with Fe (PPV of 71.4%). Between the Fe and Fe-BP groups, the highest overall accuracy of 80.0% was achieved for a combination of ki and VB. We could correctly classify 7/8 rats with Fe-BP in the defect (NPV of 86.3%) and 5/7 rats with Fe (PPV of 71.4%). Between the Fe-S and Fe-BP, the highest overall accuracy of 75.0% was achieved for a combination of VB, K1, k3, ki, and SUV. We could correctly classify 6/8 rats with Fe-BP in the defect (NPV of 75.0%) as well as 6/8 rats with Fe (PPV of 75.0%).

Discussion

In this study, 3 different classes of biomaterials, including CPC-based implants, composites of silica, and collagen and iron foam implants, were investigated using dPET-CT after they were implanted in 4-mm created rat femoral defects. CPC is a well-defined, hydroxyapatite-forming cement with a formulation based on α -tricalcium phosphate as initially described by Driessens et al. [24]. SrCOC is a strontium-enriched modification thereof, in which CaCO_3 was substituted with SrCO_3 during cement precursor fabrication [14]. This SrCPC was recently shown to enhance osteoblast precursor proliferation and osteogenic differentiation *in vitro* as well as to support new bone formation *in vivo* [15]. The 4-mm defect represented a critical-size defect with a fracture gap, which has been proven to be a good model to investigate potential bone enhancement effects of biomaterials [25]. Our data demonstrate differences in the tracer kinetics within the region of the 4-mm created defect, which includes new bone formation in the defects filled with biomaterials. For ^{18}F -Sodium fluoride, PET parameter k3 describes the formation of fluorapatite, which is indicative of new bone formation. Both CPC and SrCPC revealed statistically significant enhanced new bone formation as compared to the empty defect in the defect region [11]. However, no significant difference between the 2 different biomaterials in the defect region was detected. Recently, Ventura et al. reported PET-SUV only indicated the speed of new bone formation but not the absolute amount by correlation of PET-CT and

histology [26]. Therefore, it might be possible that PET in our study also describes the speed of new bone formation. Bone healing is a dynamic process over time, and the use of a single time point is a limitation of this study. We are considering a series of measurements in further related studies, as part of an ongoing project. In addition, in this study, SrCPC-treated animals exhibited a statistically significant higher rate of new bone formation at the biomaterial-bone interface, suggesting that a considerable amount of strontium is released from the SrCPC into the interface region and into the surrounding tissue, which are most likely related to enhanced bone formation. Recently, Andersen et al. revealed that local delivery of strontium from surface-functionalized titanium implants could increase bone-to-implant interaction for implants in the femoral shaft of healthy female Wistar rats [27]. Thormann et al. demonstrated a high Sr concentration in the interface region of the SrCPC implant by TOF-SIMS [28], which is in line with our findings. It may be concluded that strontium is released into the local milieu of osseointegrating implants, enhancing bone ingrowth into the implant surface.

Bone tissue has a highly nano-hierarchical structure, consisting mainly of collagen type I fibres and nano hydroxyapatite crystals as the matrix [29]. Scaffolds based on polymeric materials act as temporary templates for bone regeneration and actively stimulate vascularized bone growth by improving material-tissue interaction due to the porous form of the biomaterial structure [30,31]. Our results demonstrate significantly higher k_3 values of ^{18}F -sodium fluoride in the defect of rats filled with porous silicate/collagen (Sc-B30) than with silicate/collagen (B30) (Figure 3), which allows us to conclude that the formation of fluoroapatite, and therefore the new bone formation, is enhanced in the porous form of the biomaterial structure rather than in the solid form. However, a non-significant increase of k_3 in the Sc-B30Sr20 group was detected as compared with the B30 group. It is uncertain if this is caused by a lack of statistical power or by a greater degree of tissue heterogeneity than can be explained by a 2-tissue compartmental model.

References:

- Goldhahn J, Scheele WH, Mitlak BH et al: Clinical evaluation of medicinal products for acceleration of fracture healing in patients with osteoporosis. *Bone*, 2008; 43: 343–47
- Low KL, Tan SH, Zein SHS et al: Calcium phosphate-based composites as injectable bone substitute materials. *J Biomed Mater Res B Appl Biomater*, 2010; 94: 273–86
- Marie PJ: Strontium ranelate: new insights into its dual mode of action. *Bone*, 2007; 40: S5–8
- Heinemann S, Coradin T, Desimone M: Review – Bio-inspired silica-collagen materials: applications and perspectives in the medical field. *RSC Biomaterials Science*, 2013; 1: 688–702
- Desimone MF, Helary C, Mosser G et al: Fibroblast encapsulation in hybrid silica-collagen hydrogels. *J Mater Chem*, 2010; 20: 666–68
- Heinemann S, Heinemann C, Jäger M et al: Effect of silica and hydroxyapatite mineralization on the mechanical properties and the biocompatibility of nanocomposite collagen scaffolds. *ACS Appl Mater Interfaces*, 2011; 3(11): 4323–31
- Heinemann S, Coradin T, Worch H et al: Possibilities and Limitations of preparing Silica/Collagen/Hydroxyapatite Composite Xerogels as Load-Bearing Biomaterials. *Compos Sci Technol*, 2011; 71: 1873–80
- Glorius S, Nies B, Farack J et al: Metal foam-biocement composites: mechanical and biological properties and perspectives for bone implant design. *Adv Eng Mater*, 2011; 13: 1019–23
- Kałużny JJ, Grzanka D, Wisniewska A et al: Intrasclear outflow after deep sclerectomy with absorbable and non-absorbable implants in the rabbit eye. *Med Sci Monit*, 2012; 18(10): BR402–8

Recently, bisphosphonates have been a major therapeutic option in the treatment of osteoporosis. The efficacy of bisphosphonates in reducing bone resorption has been clinically estimated using biochemical indices of bone turnover [32]. Messa et al. reported a highly significant correlation ($r=0.84$) between k_1 and bone formation rate assessed by levels of serum alkaline phosphatase, as well as histomorphometry in patients with renal osteodystrophy [33]. Our results demonstrate that k_1 , which reflects bone remodeling, was significantly higher in the defect with Fe-BP than in the defect with Fe only (Figure 4). The increase of k_1 is related to the enhanced bone formation, confirming the reduced rate of bone resorption. However, a non-significant increase of k_1 in the Fe-S group was detected as compared with the Fe group.

Although we did not find further significant differences for any PET parameters between the other 2 different material groups in the defect or in the biomaterial-tissue interface region, each group could be still well classified by the combination of some parameters as measured in the defect (Table 2). It is unclear whether this is because PET is not sensitive enough for discriminating differences of bone metabolism due to the small changes of bone remodeling using different biomaterials and their enrichments, or is due to lack of statistical power.

Conclusions

With ^{18}F -sodium fluoride, k_3 was the most significant parameter for the characterization of healing processes and showed the best differentiation between the 2 different biomaterials. PET scanning using ^{18}F -sodium fluoride seems to be a sensitive and useful method for evaluation of bone healing after replacement with these biomaterials. Further studies as part of this project are ongoing.

Conflict of interest

The authors declare that they have no conflict of interest.

10. Quadbeck P, Hauser R, Kuemmel K et al: Iron based cellular metal for degradable synthetic bone replacement. PM2010 World Congress
11. Cheng C, Alt V, Dimitrakopoulou-Strauss A et al: Evaluation of different biomaterials for defect healing in an experimental osteoporotic rat model with dynamic PET-CT (dPET-CT) using F-18-Sodium Fluoride (NaF). *Injury*, 2014; 45: 501–5
12. Heiss C, Govindarajan P, Schlewitz G et al: Induction of osteoporosis with its influence on osteoporotic determinants and their interrelationships in rats by DEXA. *Med Sci Monit*, 2012; 18(6): BR199–207
13. Alt V, Thormann U, Ray S et al: A new metaphyseal bone defect model in osteoporotic rats to study biomaterials for the enhancement of bone healing in osteoporotic fractures. *Acta Biomater*, 2013; 9: 7035–42
14. Schumacher M, Henß A, Rohnke M, Gelinsky M: A novel and easy to prepare strontium (II) modified calcium phosphate bone cement with enhanced mechanical properties. *Acta Biomaterialia*, 2013; 9: 7536–44
15. Schumacher M, Lode A, Helth A, Gelinsky M: A novel strontium(II)-modified calcium phosphate bone cement stimulates hMSC proliferation and osteogenic differentiation *in vitro*. *Acta Biomaterialia*, 2013; 9: 9547–57
16. Alt V, Kögelmaier DV, Lips KS et al: Assessment of angiogenesis in osseointegration of a silica-collagen biomaterial using 3D-nano-CT. *Acta Biomater*, 2011; 7: 3773–79
17. Quadbeck P, Kümmel K, Hauser R et al: Structural and material design of open-cell powder metallurgical foams. *Advanced Engineering Materials*, 2011; 13(11): 1024–30
18. Strauss LG, Conti PS: The applications of PET in clinical oncology. *J Nucl Med*, 1991; 32: 623–48
19. Mikolajczyk K, Szabatin M, Rudnicki P et al: A JAVA environment for medical image data analysis: initial application for brain PET quantitation. *Med Inform*, 1998; 23: 207–14
20. Burger C, Buck A: Requirements and implementations of a flexible kinetic modelling tool. *J Nucl Med*, 1997; 38: 1818–23
21. Strauss LG, Pan L, Koczan D et al: Dimitrakopoulou-Strauss A. Fusion of positron emission tomography (PET) and gene array data: a new approach for the correlative analysis of molecular biological and clinical data. *IEEE Trans Med Imaging*, 2007; 26: 804–12
22. Dimitrakopoulou-Strauss A, Strauss LG, Burger C et al: On the fractal nature of dynamic positron emission tomography (PET) studies. *World J Nucl Med*, 2003; 2: 306–13
23. Cheng C, Alt V, Dimitrakopoulou-Strauss A et al: Evaluation of New Bone Formation in Normal and Osteoporotic Rats with a 3-mm Femur Defect: Functional Assessment with Dynamic PET-CT (dPET-CT) Using a 2-Deoxy-2-[18F]Fluoro-D-glucose (18F-FDG) and 18F-Fluoride. *Mol Imaging Biol*, 2012; 15: 336–44
24. Khairoun I, Boltong MG, Driessens FC, Planell JA: Effect of calcium carbonate on the compliance of an apatitic calcium phosphate bone cement. *Biomaterials*, 1997; 18: 1535–39
25. Alt V, Thormann U, Ray S et al: A new metaphyseal bone defect model in osteoporotic rats to study biomaterials for the enhancement of bone healing in osteoporotic fractures. *Acta Biomater*, 2013; 9: 7035–42
26. Ventura M, Boerman OC, Franssen GM et al: Monitoring the biological effect of BMP-2release on bone healing by PET/CT. *J Control Rel*, 2014; 183: 138–44
27. Andersen OZ, Offermanns V, Sillassen M et al: Accelerated bone ingrowth by local delivery of strontium from surface functionalized titanium implants. *Biomaterials*, 2013; 34: 5883–90
28. Thormann U, Ray S, Sommer U et al: Bone formation induced by strontium modified calcium phosphate cement in critical-size metaphyseal fracture defects in ovariectomized rats. *Biomaterials*, 2013; 34: 8589–98
29. Olsza MJ, Cheng X, Jee SS et al: Bone structure and formation: A new perspective. *Mat Sci Eng R*, 2008; 58: 77–116
30. Jones JR, Lin S, Yue S et al: Bioactive glass scaffolds for bone regeneration and their hierarchical characterisation. *J Eng in Medicine*, 2010; 224: 1373–86
31. Egli RJ, Luginbuehl R: Tissue engineering-nanomaterials in the musculoskeletal system. *Swiss Med Wkly*, 2012; 142: w13467
32. National Osteoporosis Foundation. *Clinician's Guide to Prevention and Treatment of Osteoporosis*. Washington, DC: National Osteoporosis Foundation, 2010
33. Messa C, Goodman WG, Hoh CK et al: Bone metabolic activity measured with positron emission tomography and 18F-fluoride ion in renal osteodystrophy: Correlation with bone histomorphometry. *J Clin Endocrinol Metab*, 1993; 77: 949–55